J Mater Sci: Mater Electron (2023) 34:377

Proton Bragg peak imaging by colour centre radiophotoluminescence in lithium fluoride thin film radiation detectors on silicon

R. M. Montereali[1,*], E. Nichelatti[2], V. Nigro[1], L. Picardi[1], M. Piccinini[1], A. Ampollini[1], S. Libera[1], C. Ronsivalle[1], and M. A. Vincenti[1]

[1] *Fusion and Technologies for Nuclear Safety and Security Department, ENEA C.R. Frascati, Via E. Fermi 45, Frascati, 00044 Rome, Italy*

[2] *Fusion and Technologies for Nuclear Safety and Security Department, ENEA C.R. Casaccia, Via Anguillarese 301, Santa Maria di Galeria, 00123 Rome, Italy*

Received: 19 October 2022
Accepted: 7 December 2022
Published online: 4 February 2023

ABSTRACT

Optically transparent lithium fluoride (LiF) thin films, thermally evaporated on Si(100) substrates, are under investigation as novel radiation detectors based on radiophotoluminescence for imaging of the full Bragg curves of proton beams produced by a linear accelerator for proton therapy under development at ENEA C.R. Frascati. Proton irradiation induces the formation of stable colour centres in LiF, amongst which the broadband light-emitting F_2 and F_3^+ aggregate defects, whose concentrations are locally proportional to the energy deposited in the material. Their spatial distributions in the irradiated LiF thin films and crystals are carefully measured by acquiring the latent two-dimensional visible fluorescence images with an optical microscope under blue lamp excitation. Several LiF films grown on silicon substrate were irradiated in air at increasing proton energies up to 35 MeV with their surface parallel to the particle beam and a cleaved edge perpendicularly facing it; for each sample, the fluorescence image acquired from the top surface side of the film allows to obtain the depth profile of the energy released by protons. Differences in colour centre distributions detected in LiF films with respect to LiF crystals are presented and discussed. Accurate Monte Carlo simulations allow to fully explain their experimental behaviours, paving the way towards using LiF film radiation detectors on silicon for the advanced diagnostics of proton beams at typical particle energies used for proton therapy.

Address correspondence to E-mail: rosa.montereali@enea.it

https://doi.org/10.1007/s10854-022-09770-w

1 Introduction

Passive solid-state radiation detectors based on radiophotoluminescence (RPL) in insulating materials [1], including crystals, thin films and glasses, widely utilized for radiation imaging and dosimetry [2], should feature high spatial resolution, long-term stability against fading and non-destructive reading capability.

Amongst phosphor materials, lithium fluoride (LiF) is of particular interest due to the excellent thermal and optical stability of some radiation-induced aggregate colour centres (CCs) [3], the laser-active F_3^+ and F_2 defects, consisting of two electrons bound to three and two close anion vacancies, respectively. These aggregate CCs are stable at room temperature (RT) and show distinct, broad photoluminescence emissions in the green–red spectral range under simultaneous optical excitation at about 450 nm, where they possess almost overlapping broad absorption bands, often identified as M band [4].

LiF crystals containing CCs found traditional application as passive Q-switcher optical filters and broadly tuneable solid-state lasers operating in the visible and near-infrared at RT [5]. Miniaturized light-emitting photonic devices based on optical confinement in waveguide configuration were also demonstrated [6], and F_3^+ and F_2 laser emissions were claimed in fs-inscribed distributed feedback lasers [7]. LiF thin films containing F_2 CCs were successfully used for the realization of red-emitting fully dielectric vertical microcavities [8] and of point-like sources on silicon tips for Scanning Near-Field Optical Microscopy [9]. As a matter of fact, the possibility of growing optically transparent LiF films by thermal evaporation assures a great versatility [10], thanks to the opportunity of choosing suitable substrates and geometries.

Fluorescence microscopy is a powerful and versatile technique used for the optical reading of visible RPL of atomic-scale aggregate F_3^+ and F_2 point defects, locally created in LiF crystals and thin films by lithographic techniques and different types of ionizing particles, such as low-energy electrons [10] and ion beams [11], as well as energetic photons, like X [12] and gamma rays.

The peculiar RPL properties of F_3^+ and F_2 CCs in LiF were exploited in versatile X-ray imaging detectors [13], the ones based on LiF thin films being characterized by a very high spatial resolution even for high penetrating radiations.

Recently, measurement of RPL from stable F_3^+ and F_2 radiation-induced defects, stimulated by controlled light excitation, has made undoped LiF crystals attractive also for clinical dosimetry in radiotherapy [14], because the almost tissue equivalence of this material, also well known for its use as thermoluminescent dosimeter, is essential for any meaningful application in medicine.

Hadrontherapy—cancer treatment using beams of protons or heavier ions—provides highly conformal dose delivery and greater sparing of normal tissues than conventional photon-based radiotherapy [15]. Accelerated hadrons release most of their energy per unit depth close to the end of their path in tissue, within the so-called Bragg peak, with modest lateral diffusion, thus preserving the surrounding healthy organs during tumour irradiation.

The search for novel materials and operational approaches allowing for a more precise and easier determination of the proton beam characteristics is still an active field of research. In the last years, LiF detectors based on CCs RPL in LiF crystals and thin films [16, 17] were proposed and successfully utilized also for proton beam advanced diagnostics and dosimetry [18]. In proton-irradiated LiF, the visible RPL intensity of the radiation-induced point defects has been found to be proportional to the absorbed dose over several orders of magnitude, thus novel solid-state dosimeters with imaging capabilities can be envisaged [19]. More recently, LiF crystals were also proposed and tested as novel fluorescent nuclear track detectors [20] based on F_3^+ and F_2 CCs RPL.

Above 1 MeV, accelerated protons traversing insulating materials lose their kinetic energy primarily through ionization and excitation of atoms. By adopting a suitable irradiation geometry and fluorescence microscopy as reading technique, the RPL recording of entire proton Bragg curves was successfully obtained in LiF crystals for energies from 7 [21] up to 35 MeV [22]. Thanks to the high dynamic range of proton detectors based on RPL in LiF [17], with the adoption of an analytic approach for Bragg curve modelling [23] the proton beam energy components and their spreads were estimated, even at low-dose values typical of radiotherapy [18] and in the case of multi-energetic beams [23].

In this work, the opportunity to extend this powerful approach to optically transparent LiF thin films

thermally evaporated on Si(100) substrates [24] is carefully investigated. After proton irradiation at increasing energies, performed with the film surface parallel to the particle beam propagation direction, the latent two-dimensional (2D) fluorescence images of the CCs distributions generated in the polycrystalline LiF layers show a systematic increase in the depth of the Bragg peak with respect to LiF crystals irradiated in the same conditions.

The experimental results obtained in LiF film radiation detectors on silicon at several proton energies up to 35 MeV are analysed and discussed to provide an explanation for the observed differences. Accurate Monte Carlo simulations allow to account for what is experimentally observed, paving the way towards using LiF film radiation detectors for the advanced diagnostics of proton beams at the higher particle energies used for proton therapy.

2 Experimental

2.1 Growth and characterization of LiF thin films

Polycrystalline, optically transparent LiF thin films were grown by thermal evaporation on Si(100) substrates under vacuum, at a pressure below 1 mPa, in a dedicated deposition system in the FSN-TECFIS-MNF laboratory at ENEA C.R. Frascati. The starting material consisted of LiF microcrystalline powder (Merck Suprapur, 99.99% pure), heated at ~ 850 °C in a water-cooled tantalum crucible. The LiF films have a circular shape, with a diameter of 10 mm and are deposited in the middle of Si(100) substrates, having typical dimensions $(12 \times 12)\ mm^2$ and 0.5 mm thickness, mounted on a rotating sample holder kept at a constant temperature of 300 °C during the deposition process. The evaporation rate had a fixed value of 1 nm/s, and the final thickness was automatically controlled in situ by an INFICON quartz oscillator.

The films were optically characterized by best fitting, in the spectral range extending from 190 to 1600 nm, their specular reflectance spectra measured at a Perkin-Elmer Lambda 1050 spectrophotometer. Using literature data for the extinction coefficient of Si [25], the refractive index dispersion of the substrates was obtained from reflectance spectra, measured with the same instrument, by inverting the reflectance law of a single interface separating two media of different optical constants—air and Si in the present case. As far as the LiF films are concerned, their refractive index dispersions in the visible range and other important features (thickness, surface roughness, material packing density, etc.) were estimated by best fitting their specular reflectivity spectra with a model that allows taking into account spectral changes due to film deviations from the ideally perfect thin-film model [26]. To deal with a number of measurements equal to the number of unknowns, because no transmittance measurement was possible due to Si opacity in the visible range, the extinction coefficient of the LiF films had to be assumed to be known, so that we set it to zero knowing that the typical good transparency of the deposited films is ascribable to rather negligible absorption levels.

2.2 Proton irradiation of LiF thin films and crystals

Proton beams are produced by an intensity-modulated proton linear accelerator (linac) for proton therapy under development at ENEA Frascati in the framework of the TOP-IMPLART (Oncological Therapy with Protons–Intensity Modulated Proton Linear Accelerator for RadioTherapy) project [22].

After the LiF film growth, the Si(100) substrates were cleaved in two parts to obtain a clear-cut edge covered by the LiF layer. By placing the LiF film on silicon substrate with this edge perpendicular to the proton beam direction, so that the film surface was parallel to the direction of the impinging particles (see inset in Fig. 1), the 2D fluorescence images acquired from the top LiF surface allowed to obtain the depth profiles of the energy released by protons, which has a maximum (per unit penetration length) close to the end of their path.

The irradiations were performed in air with proton beams at increasing nominal energies of 7, 18, 27 and 35 MeV. All of the LiF films were irradiated at RT. Polished LiF crystals of dimensions $(10 \times 10)\ mm^2$, 1 mm thick, were exposed to the particle beams in the same operating conditions.

A LiF film on silicon, about 0.9 μm thick, was irradiated with a proton beam of elliptic shape at a nominal energy of 7 MeV [27]. The charge per pulse was 45 pC with 25-μs long pulses at a repetition frequency of 50 Hz. The average irradiation fluence

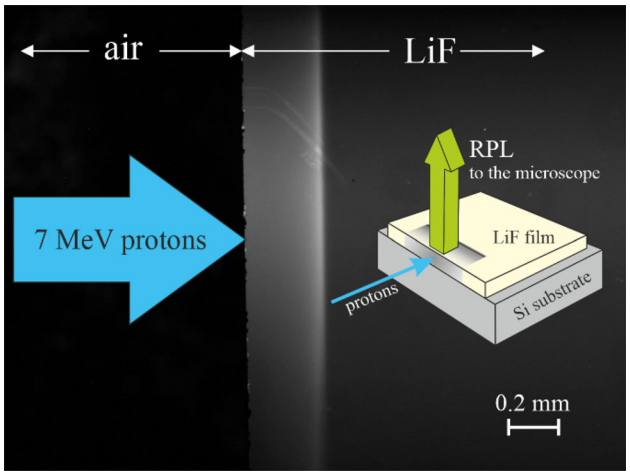

Fig. 1 RPL optical image of the top surface of a LiF film thermally evaporated on a Si(100) substrate, irradiated with a nominal 7-MeV proton beam after cleavage, acquired with the fluorescence microscope to extract the Bragg curves locally stored as distributions of stable F_3^+ and F_2 colour centres. Inset: scheme of the proton irradiation geometry for a LiF film on silicon and of RPL collection (see the text for details) (Color figure online)

was 1.1×10^{13} p/cm^2, obtained with a total number of 10^3 pulses.

Another LiF film on silicon of similar thickness was irradiated with a proton beam at a nominal energy of 18 MeV. The charge per pulse was 64 pC with 4-μs long pulses at a repetition frequency of 10 Hz. The average irradiation fluence was 5×10^{13} p/cm^2, obtained with a total number of 1.2×10^4 pulses. A LiF film grown in the same evaporation run was exposed to a multicomponent proton beam of maximum nominal energy 27 MeV in the same beam conditions of the sample irradiated at 18 MeV.

Several LiF films on silicon of higher thickness, about 1.7 μm, were irradiated with a proton beam at a nominal energy of 35 MeV. The charge per pulse was 75 pC with 4-μs long pulses at a repetition frequency of 25 Hz. The average irradiation fluence was 2×10^{13} p/cm^2, obtained with a total number of 4.2×10^3 pulses.

After proton irradiation, the RPL images stored as distributions of F_3^+ and F_2 CCs in the LiF films and crystals were read with the fluorescence microscope Nikon Eclipse 80-i, controlled by NIS Elements 4.20 software, equipped with an Hg lamp. The blue emission of the Hg lamp was optically filtered to simultaneously excite the PL of the F_2 and F_3^+ CCs and an Andor Neo sCMOS camera was used to acquire 2D optical images with 11-bit dynamic range. The RPL image analysis was performed by means of ImageJ software.

3 Results and discussion

Figure 1 shows the RPL image stored in the 0.9-μm-thick LiF film on silicon irradiated with a nominal 7-MeV proton beam at an average fluence of 1.1×10^{13} p/cm^2. A similar fluorescence image, shown in Fig. 2, is obtained from a LiF crystal irradiated in the same operating conditions of the proton accelerator.

Figure 3 shows the RPL intensity profile derived from Fig. 1 along the direction perpendicular to the film edge, obtained by image analysis of a selected horizontal portion of the luminescent vertical irradiated stripe. The spectrally integrated RPL emitted by the radiation-induced F_2 and F_3^+ CCs exhibits a strong increase at a distance from the cleaved edge of the film, which depends on the proton beam energy. Below saturation, the RPL signal depends linearly on the local defects concentration and the strong increase at a fixed distance from the exposed edge is ascribable to the Bragg peak presence. Its shape looks very similar to the experimental RPL profile obtained from a portion of the image of Fig. 2 for the LiF crystal, reported for comparison in Fig. 3. A best fit

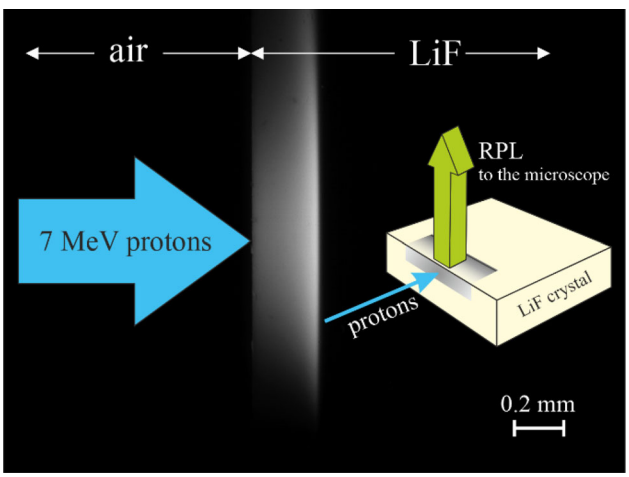

Fig. 2 RPL optical image of a polished LiF crystal, irradiated with a nominal 7-MeV proton beam, acquired with the fluorescence microscope to extract the Bragg curves locally stored as distributions of stable F_3^+ and F_2 colour centres. Inset: scheme of the proton irradiation geometry for a LiF crystal and of RPL collection (see the text for details) (Color figure online)

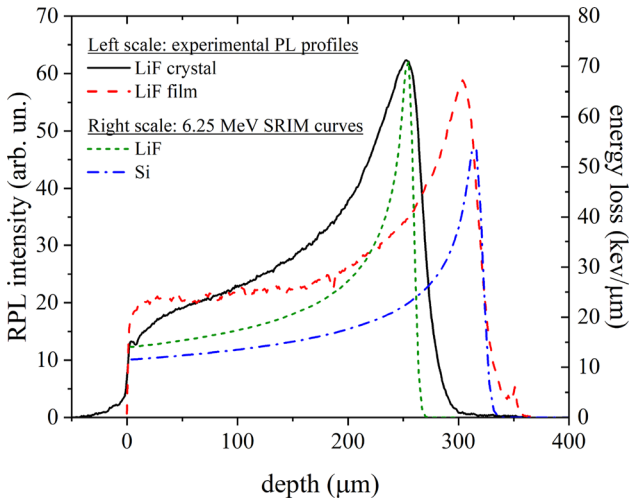

Fig. 3 Experimental RPL intensity profiles of LiF thin film (dashed) and crystal (solid) irradiated with a nominal 7-MeV proton beam compared with Bragg curves in LiF (short dashed) and Si (dash dotted), as derived from accurate SRIM simulations for a monoenergetic proton beam at 6.25 MeV

procedure applied to the RPL profiles stored in the LiF crystals, obtained for several fluences, allowed to fully reproduce them and accurately estimate the proton beam mean energy and its spread, of only 100 keV [21].

The Bragg peak position in the LiF film is found at 302 μm from the irradiated border, a distance larger than the value of 255 μm for the maximum in the LiF crystal. This maximum corresponds to the depth of the Bragg peak in LiF for a monoenergetic proton beam of 6.25 MeV, according to simulations performed with SRIM (The Stopping and Range of Ions in Matter) Monte Carlo software [28].

According to the well-known Bragg–Kleeman rule, the penetration range R, which is the mean distance travelled by protons before stopping, typically located closely behind the Bragg peak, is strongly dependent on the proton energy E

$$R = \alpha E^{p}.$$

In the formula α and p are constants, which depend on the material, in particular on its atomic number and density (2.635 g/cm^3 and 2.329 g/cm^3 for LiF and Si in the bulk form, respectively). In Fig. 3, the calculated Bragg curve is reported for a monoenergetic proton beam of 6.25 MeV in a homogeneous LiF material.

It should be highlighted that the Bragg peak depth is extremely sensitive to the material density and the polycrystalline nature of the LiF thin films could imply a reduced density of the layer, which can be considered as an aggregate of grains with void interstices [29]. As a matter of fact, it is easily understood that proton penetration length increases in a less dense material due to the less frequent interactions the particle has with the material; in quantitative terms, according to the theory, if one considers a material having a lower than 100% packing density due to presence of void interstices, an actual inverse proportionality dependence of the proton range on the material density holds true [23]. For this reason, the detected increase by ~ 16% in the depth of the Bragg peak with respect to the crystal is compatible with a ~ 16% lower material density, which means a homogeneous "porous" LiF material with a packing density of ~ 84%.

The polycrystalline LiF films thermally evaporated on Si(100) are optically transparent and, as already mentioned in Sec. 2.1, their optical constants can be estimated, together with other film parameters, from the best fit of their specular reflectance spectrum, measured before the proton irradiation. Figure 4 shows the experimental and best fitting specular reflectance spectra of the LiF thin film thermally evaporated on Si(100), from which the value of the real part of the refractive index, together with other LiF film physical parameters, could be estimated. The resulting refractive index dispersion is close to the literature data reported for a LiF crystal [30]; a

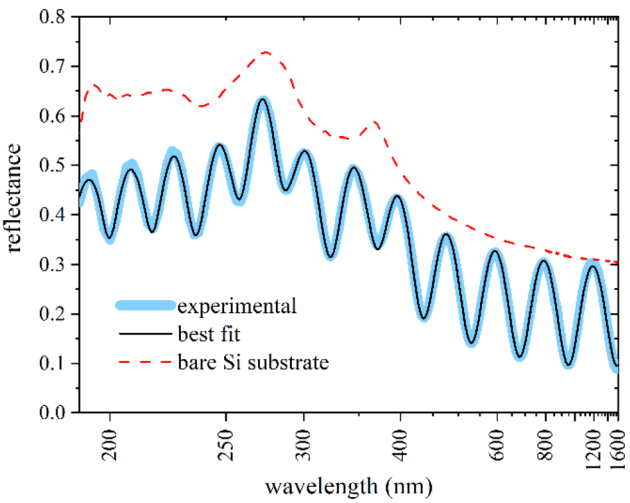

Fig. 4 Experimental and best fitting specular reflectance spectra of the LiF thin film on silicon as shown in Fig. 1. The theoretical reflectance spectrum of bare Si (dashed) is also shown for comparison

comparison with them allowed to estimate an almost negligibly lower packing density of 99.5%, which cannot explain the position difference found for the maxima in the RPL profiles of Fig. 3.

In Fig. 3 the computed Bragg curve is reported also for a monoenergetic proton beam of 6.25 MeV propagating in Si. Other phenomena, for instance, some irregularities in the cleaved edge, as well as RPL scattering and image spatial resolution, which affect the experimental RPL profiles, cannot explain the differences in the maxima positions. Saturation effects in the CCs concentration as a function of fluence can be responsible for the reduced differences between the RPL values measured at the border with air and at the maximum. Moreover, phenomena of diffusion and agglomeration of CCs are expected to modify the RPL profiles with respect to electronic energy loss in LiF crystals [11], especially in a polycrystalline LiF material irradiated at high doses [31].

To better understand the observed behaviour, a similar experiment was performed with a monoenergetic proton beam at a higher nominal energy of 18 MeV. The RPL images, stored in a LiF thin film on silicon and in a LiF crystal irradiated in the same conditions, are shown in Figs.5 and 6, respectively.

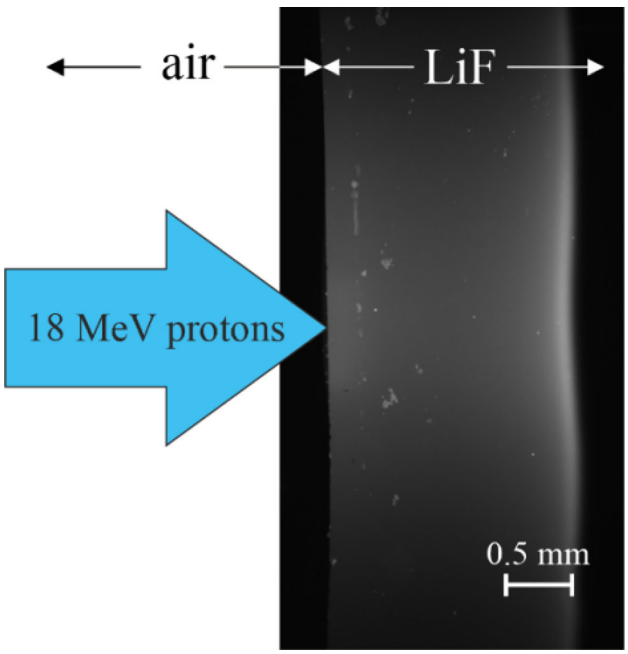

Fig. 5 RPL optical image of the top surface of a LiF film thermally evaporated on a Si(100) substrate, irradiated with a nominal 18-MeV proton beam after cleavage, acquired with the fluorescence microscope to extract the Bragg curves locally stored as distributions of stable F_3^+ and F_2 colour centres

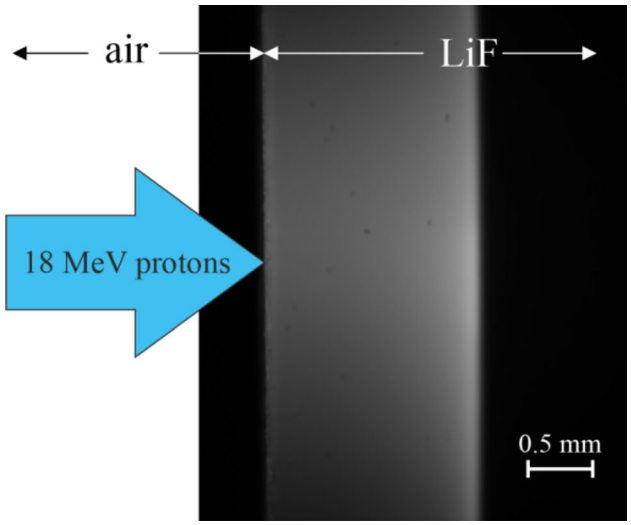

Fig. 6 RPL optical image of a polished LiF crystal, irradiated with a nominal 18-MeV proton beam, acquired with the fluorescence microscope to extract the Bragg curves locally stored as distributions of stable F_3^+ and F_2 colour centres (Color figure online)

Again, in the experimental RPL intensity profiles, reported in Fig. 7, a systematic increase in the Bragg peak by about 15% in depth was found for the LiF thin film on silicon with respect to the LiF crystal. Its value is closer to the one expected in Si rather than in LiF, as inferred from the comparison with the computed Bragg curves reported for a monoenergetic

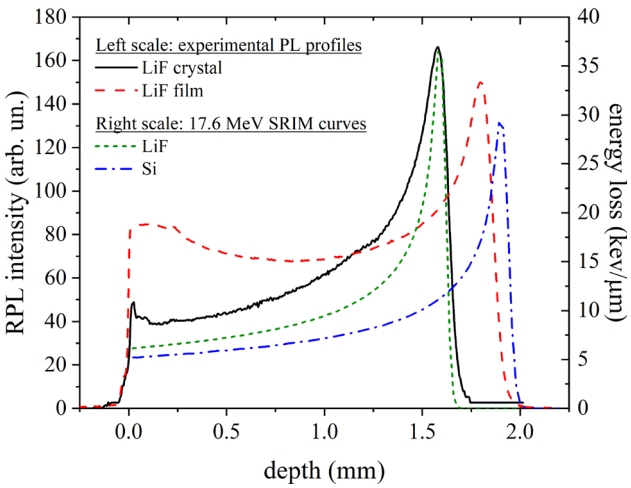

Fig. 7 Experimental RPL intensity profiles of LiF thin film (dashed) and crystal (solid) irradiated with a nominal 18-MeV proton beam compared with Bragg curves in LiF (short dashed) and Si (dash dotted), as derived from accurate SRIM simulations for a monoenergetic proton beam at 17.6 MeV

proton beam of 17.6 MeV propagating in LiF and Si, also shown in Fig. 7.

A LiF film grown in the same evaporation run, after cleavage, was exposed to a multicomponent proton beam of maximum nominal energy 27 MeV. A similar behaviour was observed for the depth of the Bragg peaks measured in this LiF film with respect to a crystal (results not shown). Also for LiF films of higher thickness, about 1.7 μm, irradiated with a 35-MeV nominal proton beam [32], systematic increases in depth of the Bragg peak with respect to crystals were observed (results not shown).

All these findings are summarized in Fig. 8, which shows the experimental Bragg peak positions measured in LiF films thermally evaporated on Si(100) compared with the penetration ranges expected in bulk LiF and Si, according to SRIM tables. In all of the LiF films, the measured depth at the peak is higher than the simulated values in bulk LiF and is closer to the ones expected in Si, that is, the substrate material.

Only accurate Monte Carlo simulations, which take into account the effects of multiple Coulomb scattering (MCS) in the layered structure constituted by the LiF thin film on the thick Si substrate, clearly demonstrate that the Bragg peaks in the films are located at the very same positions that would be expected in the underlying Si substrates rather than

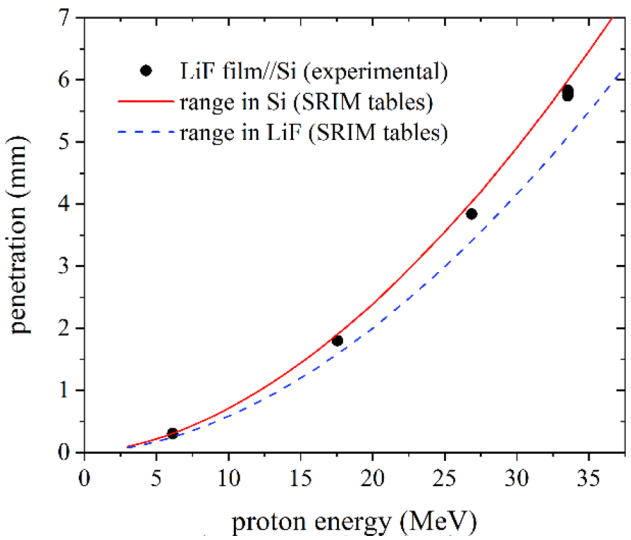

Fig. 8 Experimental Bragg peak positions (error bars smaller than the symbols) in LiF films on Si substrates for a few proton energies and expected penetration ranges in bulk LiF and Si according to SRIM tables. The plot shows that the positions of the experimental Bragg peaks closely follow the curve of Si rather than that of LiF

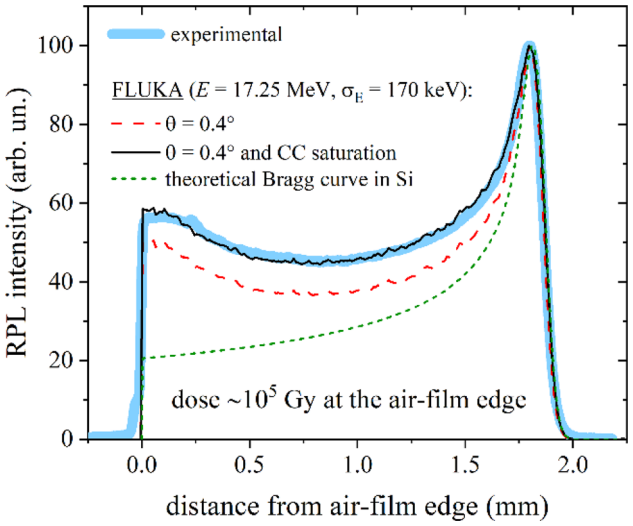

Fig. 9 RPL profile of colour centres created in a LiF film on Si substrate by irradiation with nominal 18-MeV protons. Measured profile (light-blue line) and Monte Carlo-simulated profile (black line) obtained by introducing a non-zero grazing angle and a slight saturation of the CCs density. For comparison, the simulated profile without the effect of saturation (red-dashed line) and the theoretical Bragg curve in bulk Si (green-dotted curve) are also shown (Color figure online)

in LiF [32]. The Monte Carlo simulation shown in Fig. 9 performed with FLUKA [33–35] satisfactorily reproduces the RPL profile—already shown in Fig. 7—due to CCs created in the LiF film by irradiation with nominal 18-MeV protons at the TOP-IMPLART linac in the ENEA Frascati labs. To obtain this result, several FLUKA simulations of energy deposition were run and compared, after suitable renormalisation, with the experimental RPL curve by varying simulation parameters, such as the mean energy E and standard deviation σ_E (i.e. the energy spread) of the energy spectrum, assumed to be Gaussian shaped. To get good results, it was also necessary to introduce a non-zero grazing angle of the proton beam on the sample and a small amount of saturation of the density of CCs. It was also noticed how critical the grazing angle θ is in shaping the resulting deposited energy profile; a grazing angle of + 0.4° was estimated for this case, where the plus sign stands for a proton beam impinging onto the sample from the substrate side. The most satisfying values of the simulation parameters are reported in Fig. 9. For comparison, the same figure shows the simulated curve without the effect of CC saturation and the theoretical Bragg curve in bulk Si, both

calculated with the same parameter values as the main simulation.

As far as the shape of the experimental RPL profile in Fig. 9 is concerned, one wonders why it decreases in its first part from 0 up to about 0.8 mm. We ascribe such a behaviour to the MCS of protons in the LiF film. Indeed, after entering the film, MCS causes protons to leave it soon across the film interfaces with substrate and air. An ad hoc FLUKA simulation, not reported here, of the very same proton beam and film, but without substrate (film floating in air), has shown that the proton beam fluence within the film falls to 10% of its entry value at a penetration depth of 330 μm and to 1% at 640 μm; at 0.8 mm, 99.6% of the protons that entered the film have definitely left it.

Getting back to the actual sample of Fig. 9, the above-discussed depletion of protons in the film is partially compensated by protons migrating into it from the substrate (due to MCS in the substrate), whilst a much smaller number of protons can migrate into the film from air because the low density of air—quite lighter than LiF and Si–gives rise to considerably less scattering events. Therefore, up to a depth of ∼ 0.8 mm the protons escaping the film are more than those entering it, the overall balance being an increasing loss of protons with depth, with a consequent decrease of deposited energy in the film. In agreement with the above-mentioned floating film simulation at penetration depths longer than ∼ 1 mm the protons found in the film are only those coming from the substrate. Moreover, their number increases more and more along the penetration depth because even protons in the substrate that were originally quite far from the film can reach it by continuous MCS events occurring in Si. It can be concluded that the protons giving rise to the Bragg peak in the LiF film travel most of their path in the Si substrate and travel just a modest ending fraction of it in the film. Therefore, the depth of the Bragg peak in the LiF film is reasonably much closer to that in Si than in LiF.

4 Conclusion

Although the RPL signal of visible-emitting CCs in proton-irradiated LiF films is expected to be at least one order of magnitude lower than in crystals [17], due to their limited thickness, optically transparent LiF thin films thermally evaporated on Si(100) substrates are able to store information about the proton beam energy spectrum by the local formation of radiation-induced F_2 and F_3^+ CCs with high spatial resolution (smooth profile) and a wide dynamic range on a large field of view (> 1 cm^2). At a high proton fluence and in a transverse irradiation geometry, the proton energy losses were carefully estimated from the accumulated spatial distributions of these visible-emitting aggregate defects, by reading the latent 2D fluorescence images stored in the LiF thin films with a fluorescence microscope under blue lamp excitation. The RPL profiles, measured after LiF film on silicon cleavage and irradiation in air at increasing proton energies from 7 to 35 MeV, show that the Bragg peak positions are systematically deeper than in LiF crystals. This behaviour cannot be explained with the polycrystalline nature of the LiF thin layer; rather, it is ascribable to the presence of the thick silicon substrate. The RPL profile of a cleaved LiF film on silicon, which was irradiated with an almost monoenergetic proton beam at the nominal energy of 18 MeV, shows an excellent agreement with a FLUKA simulation. The effects of MCS, taken into account by FLUKA, in both the film and the substrate allow estimating the proton beam mean energy and spread from the Bragg peak position and width, whilst the full shape of the energy loss curve has been found to be affected by the grazing angle of the proton beam with respect to the LiF film surface.

All of the presented results are very promising for the use of LiF films radiation detectors on silicon based on RPL of CCs in the advanced diagnostics of proton beams also at energies higher than those here considered and that are typical of proton therapy.

Author contributions

All authors contributed to the study conception and design. Sample preparation was performed by MAV, VN and SL. Proton irradiation of the samples was performed by CR, MP, AA and LP. Data collection was performed by MP and VN (fluorescence microscopy) and MAV and VN (spectrophotometry). Data elaboration was performed by MP and VN (photoluminescent images) and EN (photometric spectra). Simulations and best fits were performed by EN. All the work was done under the supervision and administration of RMM and LP. The first draft of the

manuscript was written by RMM and EN. All authors commented on previous versions of the manuscript. All authors read and approved the final manuscript.

Funding

Open access funding provided by Ente per le Nuove Tecnologie, l'Energia e l'Ambiente within the CRUI-CARE Agreement. This research has been carried out within the TECHEA (Technologies for Health) Project, funded by the Italian National Agency for New Technologies, Energy and Sustainable Economic Development (ENEA), Italy and the TOP-IMPLART (Oncological Therapy with Protons–Intensity Modulated Proton Linear Accelerator for Radio-Therapy) Project, funded by Regione Lazio, Italy.

Data availability

The datasets generated during and/or analysed during the current study are available from the corresponding author on reasonable request.

Declarations

Conflict of interest The authors have no relevant financial or non-financial interests to disclose.

References

1. T. Yanagida, G. Okada, T. Kato, D. Nakauchi, N. Kawaguchi, Radiat. Meas. **158**, 106847 (2022). https://doi.org/10.1016/j.radmeas.2022.106847
2. P. Olko, Radiat. Meas. **45**, 506 (2010). https://doi.org/10.1016/j.radmeas.2010.01.016
3. F. Agullo-Lopez, C.R.A. Catlow, P.D. Townsend, *Point defects in materials* (Academic Press, London, 1988), p.56
4. J. Nahum, D.A. Wiegand, Phys. Rev. **154**, 817 (1967). https://doi.org/10.1103/PhysRev.154.817
5. T.T. Basiev, S.B. Mirov, V.V. Osiko, IEEE J. Quantum Electron. **24**, 1052 (1988). https://doi.org/10.1109/3.229
6. R.M. Montereali, M. Piccinini, E. Burattini, Appl. Phys. Lett. **78**, 4082 (2001). https://doi.org/10.1063/1.1381568
7. T. Kurobori, Y. Obayashi, K. Suzuki, Y. Hirose, T. Sakai, S. Aoshima, Jpn. J. Appl. Phys. **47**, 685 (2008). https://doi.org/10.1143/JJAP.47.685
8. A. Belarouci, F. Menchini, H. Rigneault, B. Jacquier, R.M. Montereali, F. Somma, P. Moretti, M. Cathelinaud, Opt. Mater. **16**, 63 (2001). https://doi.org/10.1016/S0925-3467(00)00060-4
9. S.K. Sekatskii, G. Dietler, F. Bonfigli, S. Loreti, T. Marolo, R.M. Montereali, J. Lumin. **122–123**, 362 (2007). https://doi.org/10.1016/j.jlumin.2006.01.190
10. R.M. Montereali, Ferroelectric and dielectric thin films, in *Handbook of thin film materials*. ed. by H.S. Nalwa (Academic Press, San Diego, 2002), p.399
11. V. Mussi, F. Somma, P. Moretti, J. Mugnier, B. Jacquier, R.M. Montereali, E. Nichelatti, Appl. Phys. Lett. **82**, 3886 (2003). https://doi.org/10.1063/1.1577822
12. R. Larciprete, L. Gregoratti, M. Danailov, M. Kiskinova, R.M. Montereali, F. Bonfigli, Appl. Phys. Lett. **80**(20), 3862 (2002). https://doi.org/10.1063/1.1502906
13. G. Baldacchini, S. Bollanti, F. Bonfigli, F. Flora, P. Di Lazzaro, A. Lai, T. Marolo, R.M. Montereali, D. Murra, A. Faenov, T. Pikuz, E. Nichelatti, G. Tomassetti, A. Reale, L. Reale, A. Ritucci, T. Limongi, L. Palladino, M. Francucci, S. Martellucci, G. Petrocelli, Rev. Sci. Instrum. **76**, 113104 (2005). https://doi.org/10.1063/1.2130930
14. J.E. Villarreal-Barajas, M. Piccinini, M.A. Vincenti, F. Bonfigli, R. Khan, R.M. Montereali, I.O.P. Conf, IOP Conf. Ser. Mater. Sci. Eng. **80**, 12020 (2015). https://doi.org/10.1088/1757-899X/80/1/012020
15. H. Paganetti, *Proton therapy physics* (CRC Press, Boca Raton, 2011)
16. M. Piccinini, F. Ambrosini, A. Ampollini, L. Picardi, C. Ronsivalle, F. Bonfigli, S. Libera, E. Nichelatti, M.A. Vincenti, R.M. Montereali, Appl. Phys. Lett. **106**, 261108 (2015). https://doi.org/10.1063/1.4923403

17. M. Piccinini, F. Ambrosini, A. Ampollini, M. Carpanese, L. Picardi, C. Ronsivalle, F. Bonfigli, S. Libera, M.A. Vincenti, R.M. Montereali, J. Lumin. **156**, 170 (2014). https://doi.org/10.1016/j.jlumin.2014.08.008
18. M. Piccinini, E. Nichelatti, A. Ampollini, G. Bazzano, C. De Angelis, S. Della Monaca, P. Nenzi, L. Picardi, C. Ronsivalle, V. Surrenti, E. Trinca, M. Vadrucci, M.A. Vincenti, R.M. Montereali, Radiat. Meas. **133**, 106275 (2020). https://doi.org/10.1016/j.radmeas.2020.106275
19. R.M. Montereali, E. Nichelatti, V. Nigro, M. Piccinini, M.A. Vincenti, ECS J. Solid State Sci. Technol. **10**, 116001 (2021). https://doi.org/10.1149/2162-8777/ac31cc
20. P. Bilski, B. Marczewska, W. Gieszczyk, M. Kłosowski, T. Nowak, M. Naruszewicz, Radiat. Prot. Dosim. **178**, 337 (2018). https://doi.org/10.1093/rpd/ncx116
21. E. Nichelatti, M. Piccinini, A. Ampollini, L. Picardi, C. Ronsivalle, F. Bonfigli, M.A. Vincenti, R.M. Montereali, EPL **120**, 56003 (2017). https://doi.org/10.1209/0295-5075/120/56003
22. L. Picardi, A. Ampollini, G. Bazzano, E. Cisbani, F. Ghio, R.M. Montereali, P. Nenzi, M. Piccinini, C. Ronsivalle, F. Santavenere, V. Surrenti, E. Trinca, M. Vadrucci, E.T. Wembe, Phys. Rev. Accel. Beams **23**, 020102 (2020). https://doi.org/10.1103/PhysRevAccelBeams.23.020102
23. E. Nichelatti, C. Ronsivalle, M. Piccinini, L. Picardi, R.M. Montereali, Nucl. Instrum. Methods Phys. Res. B **446**, 29 (2019). https://doi.org/10.1016/j.nimb.2019.03.026
24. M.A. Vincenti, M. Leoncini, S. Libera, A. Ampollini, A. Mancini, E. Nichelatti, V. Nigro, L. Picardi, M. Piccinini, C. Ronsivalle, A. Rufoloni, R.M. Montereali, Opt. Mater. **119**, 111376 (2021). https://doi.org/10.1016/j.optmat.2021.111376
25. D.F. Edwards, Silicon (Si), in *Handbook of optical constants of solids*. ed. by E.D. Palik (Academic Press, San Diego, 1998), pp.547–569
26. M. Montecchi, R.M. Montereali, E. Nichelatti, Thin Solid Films **402**, 311 (2002). https://doi.org/10.1016/S0040-6090(01)01718-7
27. R.M. Montereali, A. Ampollini, L. Picardi, C. Ronsivalle, F. Bonfigli, S. Libera, E. Nichelatti, M. Piccinini, M.A. Vincenti, IOP Conf. Ser.: Mater. Sci. Eng. **169**, 012012 (2017). https://doi.org/10.1088/1757-899X/169/1/012012
28. J.F. Ziegler, M.D. Ziegler, J.P. Biersack, Nucl. Instrum. Methods Phys. Res. B **268**, 1818 (2010). https://doi.org/10.1016/j.nimb.2010.02.091
29. H.K. Pulker, Appl. Opt. **18**, 1969 (1979). https://doi.org/10.1364/AO.18.001969
30. E.D. Palik, W.R. Hunter, Lithium fluoride (LiF), in *Handbook of optical constants of solids*. ed. by E.D. Palik (Academic Press, San Diego, 1998), pp.675–693
31. M. Kumar, F. Singh, S.A. Khan, V. Baranwal, S. Kumar, D.C. Agarwal, A.M. Siddqui, A. Tripathy, A. Gupta, D.K. Avasthi, A.C. Pandey, J. Phys. D: Appl. Phys. **38**, 637 (2005). https://doi.org/10.1088/0022-3727/38/4/018
32. E. Nichelatti, V. Nigro, M. Piccinini, M.A. Vincenti, A. Ampollini, L. Picardi, C. Ronsivalle, R.M. Montereali, J. Appl. Phys. **132**, 014501 (2022). https://doi.org/10.1063/5.0098769
33. G. Battistoni, T. Boehlen, F. Cerutti, P.W. Chin, L.S. Esposito, A. Fassò, A. Ferrari, A. Lechner, A. Empl, A. Mairani, A. Mereghetti, P. Garcia Ortega, J. Ranft, S. Roesler, P.R. Sala, V. Vlachoudis, G. Smirnov, Ann. Nucl. Energy **82**, 10 (2015). https://doi.org/10.1016/j.anucene.2014.11.007
34. C. Ahdida, D. Bozzato, D. Calzolari, F. Cerutti, N. Charitonidis, A. Cimmino, A. Coronetti, G.L. D'Alessandro, A. Donadon Servelle, L.S. Esposito, R. Froeschl, R. García Alía, A. Gerbershagen, S. Gilardoni, D. Horváth, G. Hugo, A. Infantino, V. Kouskoura, A. Lechner, B. Lefebvre, G. Lerner, M. Magistris, A. Manousos, G. Moryc, F. Ogallar Ruiz, F. Pozzi, D. Prelipcean, S. Roesler, R. Rossi, M. Sabaté Gilarte, F. Salvat Pujol, P. Schoofs, V. Stránský, C. Theis, A. Tsinganis, R. Versaci, V. Vlachoudis, A. Waets, M. Widorski, Front Phys. **9**, 788253 (2022). https://doi.org/10.3389/fphy.2021.788253
35. V. Vlachoudis, FLAIR: a powerful but user friendly graphical interface for FLUKA, in *Proc. Int. Conf. on mathematics computational methods & reactor physics (M&C 2009)*. (Saratoga Springs, New York, 2009), p.2009